Fluorescence from Azobenzene Functionalized Poly(propylene imine) Dendrimers in Self-Assembled Supramolecular Structures

K. Tsuda,[†] G.C. Dol,[†] T. Gensch,[†] J. Hofkens,[†] L. Latterini,[†] J.W. Weener,[‡] E.W. Meijer,[‡] and F.C. De Schryver*[,†]

Contribution from the Department of Chemistry, Katholieke Universiteit Leuven, Celestijnenlaan 200F, 3001 Heverlee, Belgium ([†]) and the Laboratory of Macromolecular and Organic Chemistry, Eindhoven University of Technology, P.O. Box 513, 5600 MB Eindhoven, The Netherlands ([‡])

Received June 11, 1999. Revised Manuscript Received November 22, 1999

Abstract: Higher generations of poly(propylene imine) dendrimers functionalized with aliphatic chains form large micrometer-sized spherical objects in aqueous solution below pH 8. These spheres are giant vesicles with a multilaminar onion-like structure. The size distribution and the structure of the vesicles depend on the pH of the solution and the endgroups at the periphery of the dendrimer. The vesicles containing azobenzene units (**2** and **3**) fluoresce with a maximum at $\lambda_{max} = 600$ nm. This emission can be attributed to the dense and ordered arrangement of the azobenzene chromophores in the bilayer structure. Laser irradiation of a small area of giant vesicles of **2** or **3** with 1064 and/or 420 nm light leads to changes in the morphology of the vesicles. Infrared light induces a rearrangement, whereas the azobenzene units isomerize under the influence of 420 nm light. Both irradiations lead to a change in refractive index in the illuminated area. Irradiation using 420 nm light is accompanied by an increase in the emission intensity. In aqueous solutions at pH 1, the increase in fluorescence intensity is concurrent with a blue shift of the emission maximum to 540 nm. This blue shift is not observed when the experiment is performed in Milli Q water (pH 5.5). The enhanced fluorescence can be attributed to reorganization of the chromophores within the giant vesicle. The increase in emission proves that the giant vesicle is a kinetically formed system that reaches a thermodynamically more relaxed state after light-induced isomerization.

Introduction

Dendrimers are highly branched, well-defined macromolecules with a number of interesting characteristics.[1,2] Some examples of their potential use are drug delivery and nanoscale building blocks. Aggregates of dendrimers may serve as micelle mimics and, more generally, as models for biomembranes.[3] If substituted with chromophores, the highly defined and specific structure of dendrimers equip them with unique possibilities in photophysical and photochemical studies.[4−6]

The ease of controlling the position, number, interaction, and/or environment of photoactive groups at the periphery of the dendimer may lead to the development of novel photosystems. Compounds that mimick the light-harvesting complexes of photosynthesis, have efficient light absorption, and excitation-transfer to a central chromophore are an example of such systems.[7−9] There have been several attempts to synthesize supramolecular architectures with the photoisomerizable azobenzene group to obtain photoswitchable systems[10−12] or optical data storage devices.[13−16]

The dendrimers studied in this paper show interesting features, characterized as unimolecular inverted micelles that are able to bind charged organic dyes and to extract them from aqueous solutions.[17−19] Higher generation poly(propylene imine) dendrimers form vesicles in neutral or acidic aqueous solutions.[12] Protonation of the dendrimer induces a change in its structure and the interior goes outside. Simultaneously, the hydrophobic

* To whom correspondence should be addressed.
[†] Department of Chemistry.
[‡] Laboratory of Macromolecular and Organic Chemistry.

(1) Matthews, O. A.; Shipway, A. N.; Stoddart, J. F *Prog. Polym. Sci.* **1998**, *23*, 1−65.
(2) Fendler, J. H. *Membrane-Mimetic Approach to Advanced Materials*; Springer-Verlag: Berlin-Heidelberg, NewYork, 1994.
(3) Bosman, A. W.; Janssen, H. M.; Meijer, E. W. *Chem. Rev.* **1999**, *99*, 9, 1665−1688.
(4) Gensch, T.; Hofkens, J.; Hermann, A.; Tsuda, K.; Verheijen, W.; Vosch, T.; Christ, T.; Basché, T.; Müllen, K.; De Schryver, F. C. *Ang. Chem. Int. Ed. Engl.* **1999**, *38*, 3752−3756.
(5) Hofkens, J.; Latterini, L.; De Belder, G.; Gensch, T.; Maus, M.; Vosch, T.; Karni, Y.; Schweitzer, G.; De Schryver, F. C.; Hermann, A.; Müllen, K. *Chem. Phys. Lett.* **1999**, *304*, 1−9.
(6) Ringsdorf, H.; Schlarb, B.; Venzmer, J. *Angew. Chem., Int. Ed. Engl.* **1988**, *27*, 113.
(7) Jiang, D. L.; Aida, T. *Nature* **1997**, *388*, 454−456.
(8) McElhanon, J. R.; Wu, M. J.; Escobar, M.; Chaudry, U.; Hu, C. L.; McGrath, D. V. *J. Org. Chem.* **1997**, *62*, 908−915.
(9) Swallen, S. F.; Shi, Z. Y.; Tan, W. H.; Xu, Z. F.; Moore, J. S.; Kopelman, R. *Luminescence* **1998**, *76*, 193−196.
(10) Archut, A.; Vögtle, F.; De Cola, L.; Azzelini, G. C.; Balzani, V.; Ramanujam, P. S.; Berg, R. H. *Chem. Eur. J.* **1998**, *4*, 699−706.
(11) Archut, A.; Azzelini, G. C.; Balzani, V.; De Cola, L.; Vögtle, F. *J. Am. Chem. Soc.* **1998**, *120*, 12 187−12 191.
(12) Schenning, A. P. H. J.; Elissen-Roman, C.; Weener, J. W.; Baars, M. W. P. L.; van der Gaast, S. J.; Meijer, E. W. *J. Am. Chem. Soc.* **1998**, *120*, 8199−8208.
(13) Tripathy, S.; Kim, D.-Y.; Li, L.; Kumar, J. *Pure Appl. Chem.* **1998**, *70*, 1267−1270.
(14) Zilker, S. J.; Bieringer, T.; Haarer, D.; Stein, R. S.; van Egmond, J. W.; Kostromine, S. G. *Adv. Mater.* **1998**, *10*, 855−859.
(15) Meng, X.; Natansohn, A. *Polymer* **1997**, *38*, 2677−2682.
(16) Buffeteau, T.; Labarthet, F. L.; Pézolet, M.; Sourisseau, C. *Macromolecules* **1998**, *31*, 7312−7320.
(17) Baars, M. W. P. L.; Froehling, P. E.; Meijer, E. W. *J. Chem. Soc., Chem. Commun.* **1997**, *20*, 1959−1960.
(18) Jansen, J. F. G.; de-Brabander-van den Berg, E. M. M.; Meijer, E. W. *Science* **1997**, *266*, 1226−1229.
(19) Stevelmans, S.; Van Hest, J. C. M.; Jansen, J. F. G. A.; Van Boxtel, D. A. F. J.; Vandenberg, E. M. M. D.; Meijer, E. W. *J. Am. Chem. Soc.* **1996**, *118*, 7398−7399.

10.1021/ja9919581 CCC: $19.00
Published on Web 03/28/2000

chains come together and form well-packed bilayers in which the alkyl chains are oriented parallel to each other.

We found that the vesicles containing azobenzene groups (**2** and **3**) can also be visualized by fluorescence microscopy using 420 nm laser light. In this paper we report a study of the properties of 5th generation poly(propylene imine) dendrimers **1**, **2**, and **3**, which are decorated with side chains containing 64 palmitoyl, 32 palmitoyl and 32 azobenzene, and 64 azobenzene groups, respectively. The parameters of importance for vesicle formation and the influence of organization in the assembled bilayer structures on the fluorescence emission were investigated.

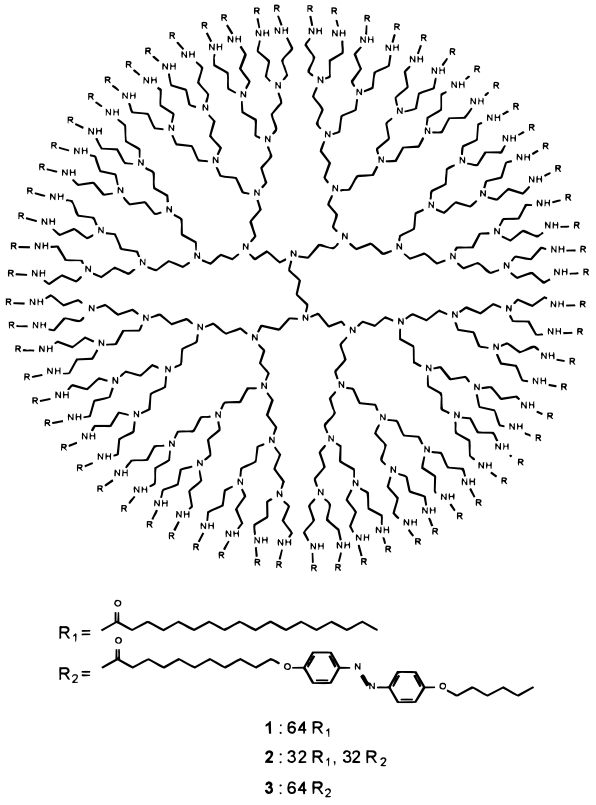

Results

Size Distribution. Compounds **1**−**3** form spherical vesicles with diameters up to 22 μm when a solution of the dendrimer in tetrahydrofuran (THF) is injected in aqueous solutions (buffered at pH 1). The obtained, opalescent solutions were studied using transmission and fluorescence microscopy. In Figures 1A and B, typical transmission microscopy images of vesicles dispersions are shown. The diameters and size distribution of the giant vesicles were determined from 50 transmission images (Figures 1C and 1D). The number in the lowest bin (0−0.5 μm) is underestimated due to resolution limits (i.e., particles $<$0.5 μm cannot be measured properly). The mean value and the maximum size of the vesicles are shown in Table 1. The size distribution of the vesicles from the dendrimer with palmitoyl groups only (**1**) has a peak $\sim$1 μm and extends substantially to larger sizes. Increasing the content of azobenzene units (**2** and **3**) leads to the formation of objects with a larger diameter (see Table 1). The diameter mean size (d_{av}) and the maximum size (d_{max}) of the azobenzene-containing vesicles are clearly shifted to a larger size (see Table 1). For example, dendrimer **3** yields vesicles with a d_{av} of 2.4 μm, whereas dendrimer **1** affords vesicles with an average diameter of 1.9 μm. In all samples, a small fraction of the vesicles are $>$10 μm in diameter; the largest ones found are 22 μm in diameter.

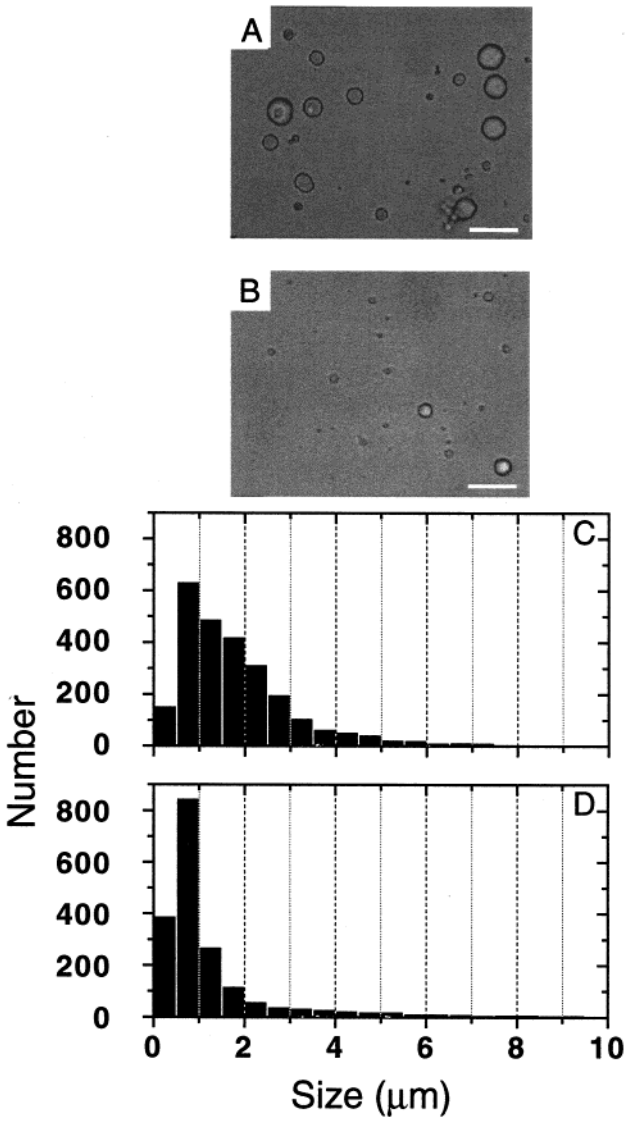

Figure 1. Transmission microscopy images of giant vesicles of **2** at pH 1 (A) and pH 5.5 (B). The respective size distribution histograms of the vesicles are shown in C and D. The size of scale bars is 10 μm.

Table 1. Mean (d_{av}) and Maximum (d_{max}) Diameter of Giant Vesicles Obtained from Transmission Microscopy Images

compound	solution	d_{av}, μm	d_{max}, μm
1	pH 1	1.9	13
2	pH 1	2.2	15
3	pH 1	2.4	22
2	Milli Q	1.5	14

When a solution of **2** was injected in Milli Q water of pH 5.5, spherical objects were still formed. However, the average diameter strongly shifted to a smaller value compared with the experiments at pH 1 (see Figures 1C and 1D, and Table 1).

A more detailed analysis of the transmission images of vesicles of **1** and **2** gave the impression that most are homogeneous and do not contain substructures (Figure 2). However, a few vesicles, especially the ones $>$5 μm, displayed domains with a different refractive index inside the vesicle (Figure 3). These substructures were found in nearly every vesicle of **3**, which contains azobenzene groups only (image not shown).

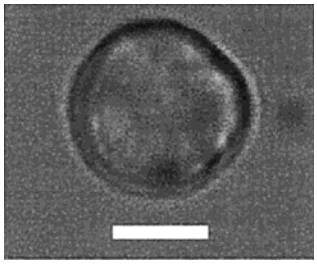

Figure 2. Transmission microscopy image of a vesicle from **2** at pH 1 without substructures. The size of the scale bar is 5 μm.

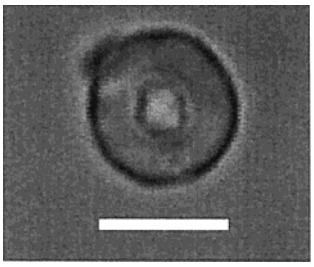

Figure 3. Transmission microscopy image of a vesicle from **2** at pH 1 with a substructure. The size of the scale bar is 5 μm.

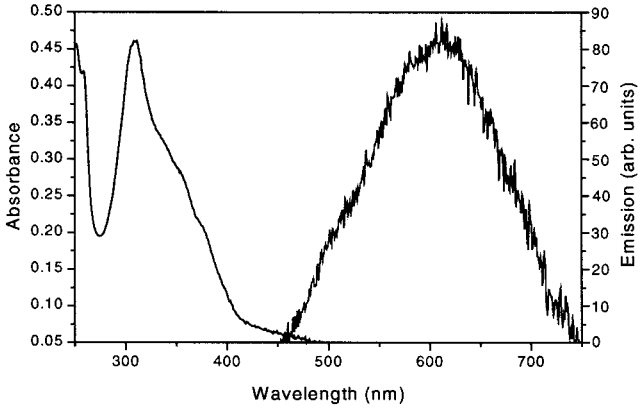

Figure 4. Absorption and emission spectra (λ_{ex} = 400 nm) of an aqueous dispersion of vesicles of **2**, measured with a spectrophotometer.

Fluorescence Microscopy. The absorption spectrum from an ensemble of vesicles of **2**, measured with a spectrophotometer, is depicted in Figure 4. The absorption spectrum contains a broad band at 310 nm, which originates from azobenzene aggregates, and a shoulder at 360 nm, which is from the $\pi-\pi^*$ transition of the trans azobenzene units. This absorption extends to 450 nm, where the forbidden $n-\pi^*$ transition of the trans isomer is located.[20] Upon excitation between 380 and 440 nm, the emission spectrum shows a maximum centered at 600 nm.

The vesicle dispersions of the azobenzene-containing dendrimers (**2** and **3**) could also be studied using fluorescence microscopy (λ_{ex} = 420 nm). Vesicles detected by transmission microscopy (Figures 2 and 3) could also be measured using fluorescence microscopy. The emission intensity is homogeneously distributed over the giant vesicle, as shown in Figure 5, which displays a *z*-scan obtained with confocal laser scanning microscopy (CLSM). This *z*-scan is obtained for the vesicle whose transmission image is represented in Figure 2.

z-Scans of the vesicles can also be used to investigate substructures in the larger vesicles of **2** and **3**. Figure 6 shows confocal fluorescence images of a structured vesicle of **2** whose transmission image is depicted in Figure 3. From these fluorescence images it can be seen that the center of the vesicle consists of a nonfluorescent region. This region corresponds to the region with a different refractive index from its surroundings, as visualized in its transmission image (Figure 3).

(20) Rau, Von H. *Ber. Bunsen-Ges. Phys. Chem.* **1967**, *71*, 48−53.

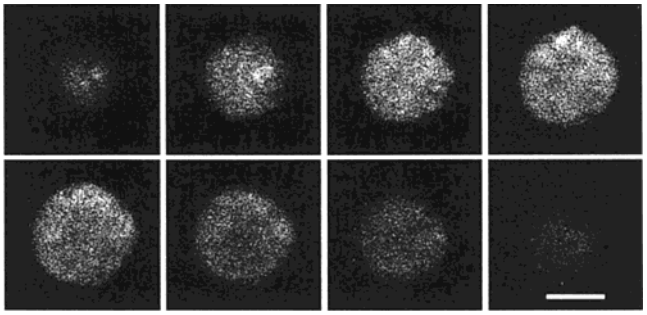

Figure 5. *z*-Series of CLSM images of a giant vesicle from **2** at pH 1 without substructures. The size of the scale bar is 5 μm. The *z*-slice size is 1 μm, starting at the lowest part of the vesicle.

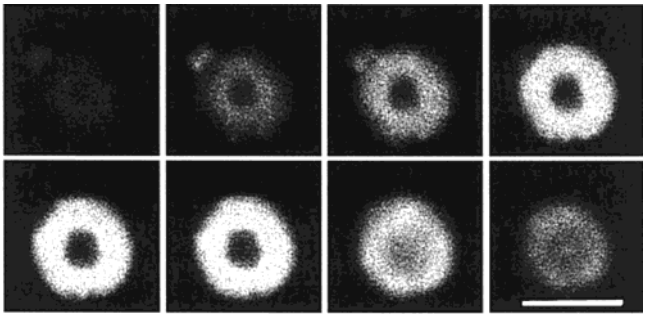

Figure 6. *z*-Series of CLSM images of a giant vesicle from **2** at pH 1 with substructures. The size of the scale bar is 5 μm. The *z*-slice size is 1 μm, starting at the lowest part of the vesicle.

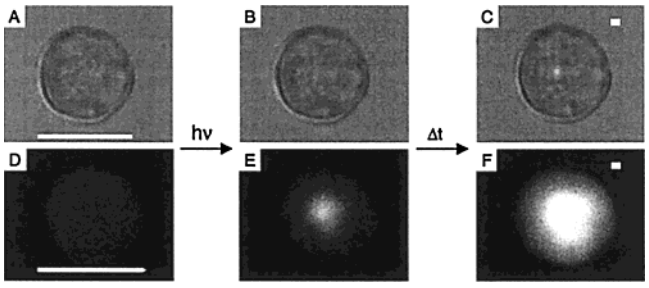

Figure 7. Transmission (A−C) microscopy and their corresponding fluorescence (D−F) images of giant vesicles from **2** in a solution of pH 1 (λ_{ex} = 420 nm): A and D, before irradiation; B and E, after 30 s of irradiation; C and F, 2 min after irradiation, respectively. The white rectangles in C and F represent the irradiated area. The size of the scale bars is 10 μm.

Fluorescence Enhancement. Irradiation of a small area of ~0.5 μm^2 in a giant vesicle for 30 s, using a focused laser beam (λ_{ex} = 420 nm), results in an increase in the emission intensity of that area (Figure 7E versus 7D). Only the long residence time of the laser light induces an increase in the emission intensity. In these experiments, the illumination time during image scanning is 16 μs for one pixel (area is 0.007 μm^2) and the average power in the diffraction-limited spot is 25 kW cm^{-2}. The beam can be positioned at a certain region of the vesicle when scanning is stopped. In this case, the illuminated spot receives ~10^6 times more light energy compared with the rest of the vesicle. If subsequently the giant vesicle is stored in the absence of light, and only imaged from time to time, a further increase in emission intensity is found (Figure 7F versus 7E). Irradiation with 420 nm laser light also alters the refractive index of the vesicle, as can be seen in Figure 7C.

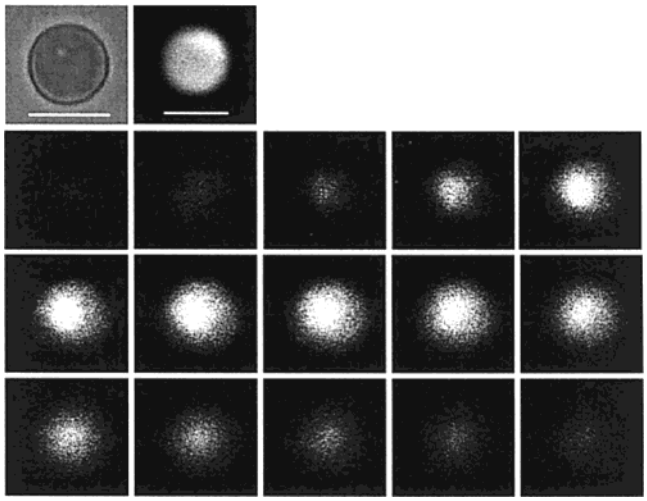

Figure 8. Top images: transmission image (left) and fluorescence image (right) of a vesicle from **2**. Confocal fluorescence image *z*-scan, after an irradiation experiment ($\lambda_{ex} = 420$ nm). The size of the scale bar is 10 μm, and the *z*-scan step size is 1 μm.

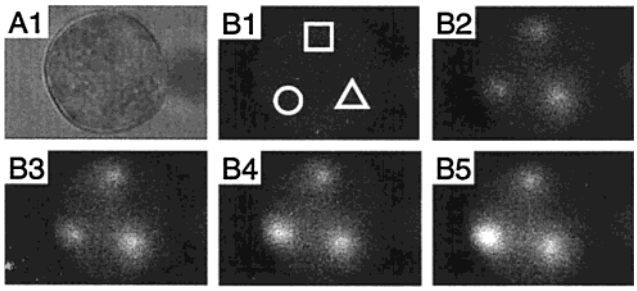

Figure 9. Fluorescence and transmission microscopy images of a giant vesicle monitored in enhancement experiments. Transmission: A1, before the irradiation. Fluorescence: B1, fluorescence before the irradiation; B2, directly after the 1st irradiation (○, 30 s; □, 30 s; △, 60 s); B3, 60 min after the 1st irradiation; B4, directly after the 2nd irradiation (○, 30 s); B5, 60 min after the 2nd irradiation. The size of the vesicle is 20 μm, $\lambda_{ex} = 420$ nm, and $P = 25$ kW cm^{-2}.

To investigate this enhancement in more detail, we illuminated a large vesicle at three different loci with the same number of photons, but delivered in different time intervals. The region on the right (△) was illuminated for 60 s, whereas the other two regions (□, ○) were illuminated for 30 s only. After 1 h, the area on the left (○) was illuminated for an additional 30 s, thereby also reaching a total irradiation of 60 s. In Figures 9B1 to 9B5, a selection of fluorescence microscopy images are shown. Figure 10 shows the corresponding fluorescence intensity of the regions (○, △, □) from Figure 9. The fluorescence images in Figure 9, as well as the intensity plots in Figure 10, show that the two regions (□, ○) illuminated for 30 s obtain the same fluorescence intensity after 1 h (2000 arbitrary units). The other region (60 s, △) grows to a much higher intensity of ∼2600 arbitrary units. After the second illumination the left-hand region (○) starts to grow in intensity and slightly exceeds the fluorescence of the region that received the 60 s of illumination at once (△). The emission of the first region (○) reached a maximum value of 2800 arbitrary units after 1 h, which is, within the experimental error, similar to the emission intensity obtained after 60 s of irradiation (2600 arbitrary units).

The emission spectra of the isolated vesicles were also recorded using a charge-coupled device (CCD)-camera coupled to a confocal fluorescence microscope.[21] Figure 11 shows the

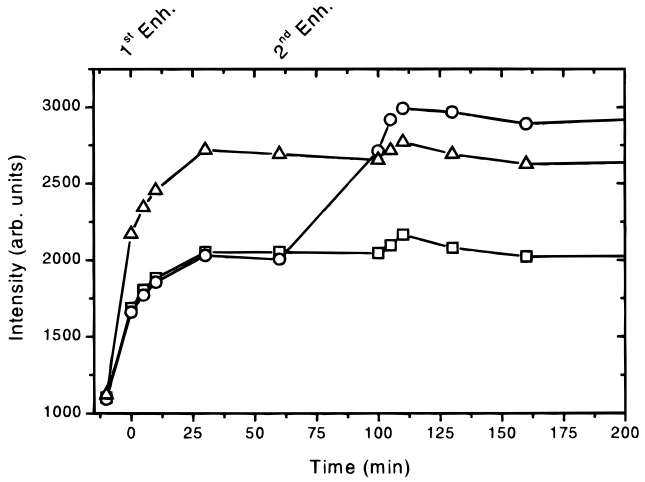

Figure 10. Plot of the intensity versus time of the enhanced regions in the vesicle from Figure 9 (△, 60 s of illumination at once; ○, 30 s of illumination + additional 30 s after 1 h; □, 30 s of illumination; $\lambda_{ex} = 420$ nm; $P = 25$ kW cm^{-2}).

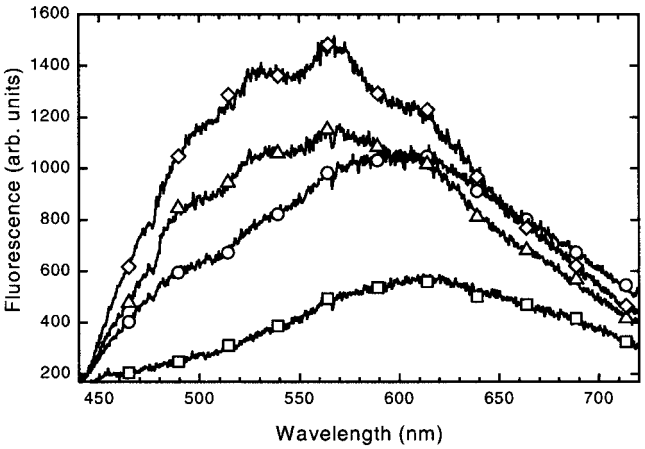

Figure 11. Emission spectra of an irradiated spot of a single giant vesicle of **2** at pH = 1: curve 1 (□, before irradiation); curve 2 (○, 60 s irradiation); curve 3 (△, 300 s irradiation); and curve 4 (◇, 300 s irradiation + 30 min dark period); $\lambda_{ex} = 420$ nm, $P = 25$ kW cm^{-2}.

typical emission spectra from giant vesicles before (□) and after a fluorescence enhancement experiment (○, △, ◇). Before irradiation, a broad single-band spectrum with a maximum at 615 nm was obtained, which is comparable to the emission from an ensemble of vesicles in an aqueous dispersion that has a maximum at 600 nm (see Figure 4).

The emission spectra taken during the fluorescence enhancement and after the subsequent storage in the absence of light (curves ○, △, and ◇ in Figure 11), show a blue shift in addition to the overall increase of intensity.

Identical experiments were performed on a dispersion of vesicles of **2** in milli-Q water (pH 5.5) instead of the tritisol buffer (pH 1). The fluorescence spectrum obtained before irradiation, shown in Figure 12 (□), is very similar to that observed at pH 1 (curve □ in Figure 11). The fluorescence intensity of these vesicles can also be enhanced, and again a further increase in intensity is observed after storage in the absence of light. However, the spectral change at the blue side is not as pronounced as the experiment at pH 1 (Figure 11)

Simultaneous Irradiation with 1064 and 420 nm Light. A morphological change could be observed when giant vesicles

(21) Gensch, T.; Hofkens, J.; van Stam, J.; Feas, H.; Creutz, S.; Tsuda, K.; Jerome, R.; Masuhara, H.; De Schryver, F. C. *J. Phys. Chem. B* **1998**, *102*, 8440−8451.

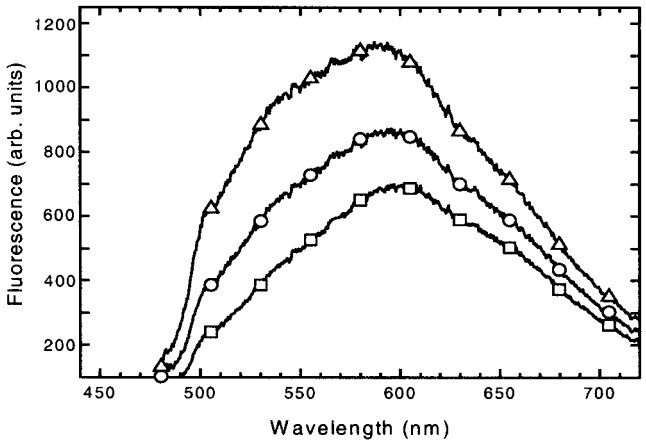

Figure 12. Emission spectra of an irradiated spot of a single giant vesicle of **2** at pH = 5.5: curve 1 (□, before irradiation); curve 2 (○, 300 s irradiation); and curve 3 (△, 300 s irradiation + 30 min dark period); λ_{ex} = 420 nm, P = 25 kW cm^{-2}.

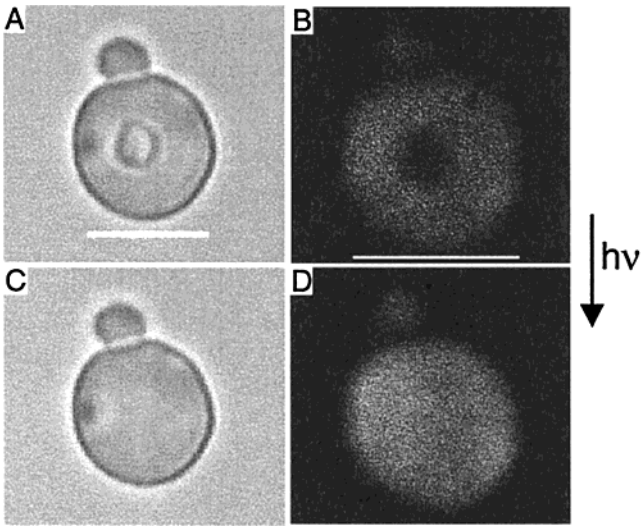

Figure 13. Transmission and fluorescence microscopy images of giant vesicles of **2** in pH 1: (A,B) before irradiation, (C,D) after simultaneous irradiation with 420 nm, P = 25 kW cm^{-2} and 1064 nm light, P = 250 MW cm^{-2}. The size of the scale bar is 5 μm.

from **2**, deposited on glass, were irradiated with a high power of infrared (IR) laser light (~250 MW cm^{-2} in the sample). Figure 13 shows the transmission and fluorescence microscopy images of a vesicle with a nonfluorescing domain, resembling the one depicted in Figure 3. After simultaneous irradiation with 1064 and 420 nm light, the substructure disappeared. The fluorescence image recorded afterward (Figure 13D) indicates that the previously dark region in emission has become fluorescent as well, suggesting that a reorganization of the vesicle occurred.

Discussion

General. Similar to previously published data,[12] the large vesicles studied in this paper consist of many bilayer structures, based on data obtained from microscopic techniques including cryo-transmission electron microscopy (TEM), scanning electron microscopy (SEM), and confocal laser scanning microscopy (CLSM). The so-called giant vesicle is a "filled sphere"; that is, a multilaminar structure with an onion-like architecture with repetitive 5-nm bilayer structures containing water molecules.[22] In this aggregate, the bilayers consist of interdigitated end-groups of the dendrimers, which are restricted in their mobility.

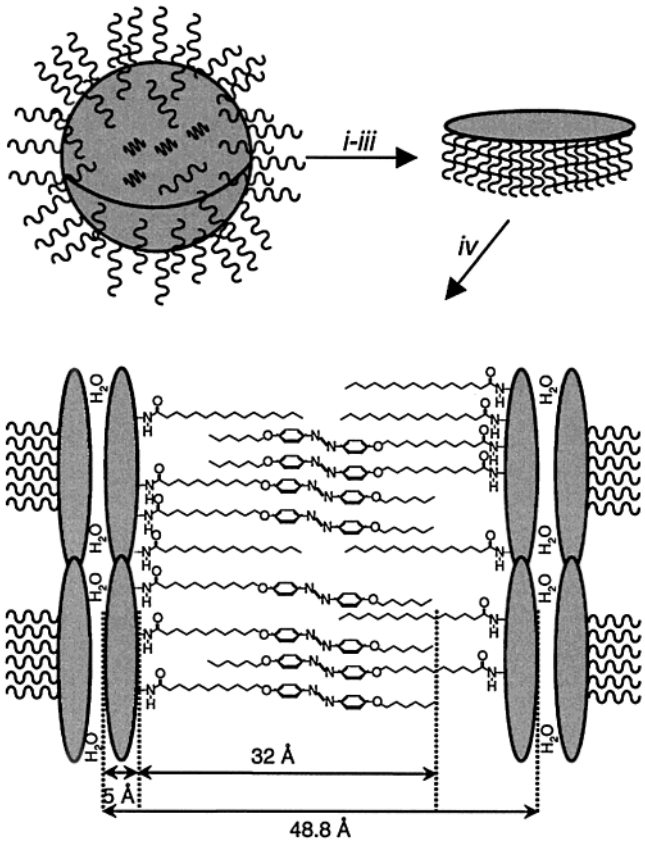

Figure 14. Illustration of the formation of the bilayer structure: (a) (*i*) injection of the dendrimer in an aqueous solution of pH < 8; (*ii*) protonation of the nitrogen atoms; (*iii*) structural inversion of the dendrimer; (*iv*) self-aggregation of the protonated dendrimers to form multilaminar vesicles containing interdigitated bilayers. This schematic representation is based on data from SAXS and cryo-TEM measurements (data published elsewhere[22]).

The highly polar, flattened cores of the dendrimers, consisting of protonated nitrogen atoms, are directed to their counterparts and separated from the next layer by an aqueous phase. It can be stated that each dendrimer resembles an aggregate of surfactants whose hydrophilic headgroups are covalently bound, thus improving the stability of the bilayer structures. Small-angle X-ray measurements (SAXS) on a dispersion of vesicles from dendrimer **1** revealed a 4.9 nm thickness for the bilayer, which agrees perfectly with our estimation from cryo-TEM (data presented elsewhere[22]). Based on the length of a fully extended alkyl chain carrying a *trans*-azobenzene unit (32 Å), we constructed the schematic representation depicted in Figure 14.

Size Distribution and Morphology of the Vesicles. The histograms displayed in Figure 1 confirm that a large variation in size can be found in vesicles made from the same dendrimer **2** but at a different pH. The pH of the solution has a pronounced effect on the size distribution of vesicles from **2**. At a pH of 5.5, there are only few giant vesicles and mainly small vesicles can be observed in transmission images. Under less acidic conditions, there is reduced protonation of the dendrimer, which diminishes the surfactant-like properties of the dendrimer and will affect the assembly of the dendrimers.

Table 1 shows that the end-groups of the dendrimer have a pronounced effect on the size of the vesicles formed. In general,

(22) Dol, G. C.; Tsuda, K.; Weener, J. W.; Bartels, M. J.; Asavei, T.; Gensch, T.; Hofkens, J.; Latterini, L.; Schenning, A. P. H. J.; Meijer E. W.; De Schryver F. C., submitted to Nature.

it can be stated that azobenzene-containing dendrimers (**2** and **3**) form larger vesicles than the palmitoyl-only dendrimer (**1**). Comparison of the d_{av} of the different vesicles shows a gradual increase going from **1** (100% palmitoyl groups) to **3** (100% azobenzene groups; see Table 1). This increase is mainly due to additional $\pi-\pi$ stacking interactions in the vesicles from **2** and **3**, which enhance the stabilization of the vesicles. Evidence for stacking can be found in the absorption spectrum (Figure 3), which contains the typical bands of azobenzene aggregates at e.g. 310 nm.[23,24]

The main difference between vesicles made from **2** and **3** is their morphology. Vesicles of **3** (azobenzene groups only) possess many more irregular substructures than the ones of **2** (mixed azobenzene and palmitoyl groups). The high number of azobenzene units in **3** might lead to the formation of crystalline domains.

Fluorescence Microscopy. Fluorescence microcopy is a suitable tool to visualize vesicles from **2** and **3**. The *z*-scans obtained using CLSM show that the emission intensity is distributed homogeneously over most of the vesicles. This result is an indication that the vesicles are filled spheres (i.e., they consist of dendrimer throughout the whole sphere). The latter is confirmed by the images displayed in Figure 8, which shows that enhancement occurs in every confocal *z*-slice, proving the filled-sphere character of the vesicle. This result is in agreement with the previously suggested onion-like organization of bilayers. The experiment was repeated several times on different vesicles to verify the initial "steady state" of fluorescence and the position of the enhanced region, which was identical in all experiments. Vesicles of **3** behaved similar to those of **2**.

Fluorescence Enhancement. Irradiation with 420 nm light leads to an increase of the fluorescence intensity, as shown in Figures 7−10. We propose that this intensity increase is caused by trans−cis isomerizations taking place in the organized bilayer structure. It has been reported that visible light in the range of 436 to 514 nm can induce photoisomerizations in azobenzene. It has to be noted, however, that the amount of *cis*-azobenzene produced by visible light is much lower than that produced by ultraviolet (UV) light (e.g., 360 nm).[25] In our case, irradiation at 420 nm laser light also induces trans-to-cis and cis-to-trans photoisomerization cycles, followed by reorientation of azobenzene moieties. It is well known that linearly polarized laser light can induce reorientation of azobenzene groups through photochemical isomerizations.[26] The reorganization leads to a different state of aggregation, resulting in an increase in fluorescence intensity and a different refractive index. This latter phenomenon has found applications in the field of optical data storage.[10,13−15, 27]

The change in refractive index can be seen in Figure 7C, which shows a different contrast in the transmission image compared with that in Figure 7A. The area with the altered refractive index is comparable to the actual irradiated area (white rectangle in Figure 7C). The area with the enhanced fluorescence intensity, on the other hand, is much larger than the irradiated area (white rectangle in Figure 7F). The cause of this apparent discrepancy is the spatially "nonselective" excitation of the focused laser. The dumbbell shape of the excitation laser beam leads to a fluorescence enhancement in *z*-layers far from the focus. The out-of-focus regions are larger than the diffraction-limited focal spot, with a radius of 210 nm. Both in the upper and lower region, photoisomerizations are also induced, although the irradiation intensity in the out-of-focus region is lower than at the focal point.

In Figure 8, the confocal *z*-scan of a vesicle after fluorescence enhancement shows that the enhancement occurs throughout the whole vesicle. In this case, 15 *z*-slices of 1 μm were recorded for a vesicle with a diameter of 10 μm. This might suggest that the vesicle has an oval shape. However, because of a refractive index mismatch between immersion oil, medium (water), and the vesicles, the number of *z*-slices needed to image the vesicles is incorrect. We calibrated our setup using Focal check samples, obtained from Molecular Probes. A bead of 15 μm required 25 *z*-slices to determine the axial distance. Using this calibration factor of 0.667 μm/*z*-slice results in an axial diameter of ∼9 μm for the vesicle depicted in Figure 8, which is close to the diameter determined from the transmission image.

The irradiation experiments performed on the giant vesicle, depicted in Figure 9, indicate that the enhancement is a dynamic process. The right-hand region, with 60 s of illumination (△) at once, receives a large amount of photons and has reached a "relaxed" state after ∼30 min. The region on the left (○) received the total of 60 s of illumination, but delivered in two separated portions. Figure 9 shows that the emission intensity of the two regions (△ and ○) reaches approximately the same value (2700 arbitrary units), which is an increase of a factor 2.7. This result indicates that the time interval in which the photons are absorbed is of minor importance. Only the amount of photons determines the total increase of fluorescence. The top region (□), which received only 30 s of illumination, reaches an intensity of 2000 arbitrary units, which is an increase of a factor 2. The small decrease in intensity after 120 min is caused by changes in the focus of the microscope.

Simultaneous Irradiation with 1064 and 420 nm Light. The effect of the interactions of the vesicles with IR light, shown in Figure 13, is caused by the "heat mode" of interaction. The heat mode is indirectly caused by the absorption of light by water molecules, which have a minor absorption at 1064 nm due to an overtone.[28] To prove this hypothesis, we performed the same experiments in D_2O, which does not absorb IR light of 1064 nm. In these experiments, the morphology of the vesicles remained unaltered, proving that the locally generated heat is responsible for the changes observed in H_2O. Additionally, these experiments prove the presence of water (H_2O or D_2O) in the vesicles, supporting the idea that water separates two bilayers. If water molecules are incorporated in the bilayer framework, the formed heat cannot be convected. The rise in temperature increases the mobility and leads to a change in morphology.

Simultaneous irradiation with IR light (heat formation) and blue light (isomerization cycling) induces the disappearance of nonfluorescent domains, as shown in Figure 13C and 13D. This feature could not be observed when either of the two light sources was applied separately. In the literature, it is reported that efficient photoisomerization first enhances the mobility in azobenzene-functionalized polymeric material. After the initial softening, the back-isomerization, accompanied by reorganization, causes a plasticizing or hardening of the material.[29] The

(23) Shimomura, M.; Kunitake, T. *J. Am. Chem. Soc.* **1987**, *109*, 5175−5183.
(24) Shimomura, M.; Ando, R.; Kunitake, T. *Ber. Bunsen-Ges. Phys. Chem.* **1983**, *87*, 1134−1143.
(25) Wu, Y.; Zhang, Q.; Kanazawa, A.; Shino, T.; Ikeda, T.; Nagase, Y. *Macromolecules* **1999**, *32*, 3951−3956.
(26) Eich, M.; Wendorff, J. H. *Makromol. Chem. Rapid Commun.* **1987**, *8*, 467−471.
(27) Holme, N. C. R.; Ramanujam, P. S.; Hvilsted, S. *Opt. Lett.* **1996**, *21*, 902−904.
(28) Svoboda, K.; Block, S. M. *Annu. Rev. Biophys. Biomol. Struct.* **1994**, *23*, 247−285.
(29) Bohm, N.; Materny, A.; Kerfer, W.; Steins, H.; Muller, M. M.; Schottner, G. *Macromolecules* **1996**, *29*, 2599

photoisomerization involves a structural rearrangement in the azobenzene chromophores, producing sterical pressure and electronic interactions that might force changes in the local structure of the bilayer. But, as mentioned previously, the stability of the bilayer in our case is so high that additional energy is needed to achieve morphological changes. In this case, the required energy is introduced indirectly by IR light so that reorganization can occur to its full extent.[30,31]

Photophysical Aspects. The azobenzene chromophore presents reversible photochromism based on its trans−cis photoisomerization. In the literature, extensive experimental and theoretical studies have been carried out to elucidate the properties and deactivation mechanism of the azobenzene unit.[32] The trans isomer is thermodynamically more stable (∼56 kJ/mol), but the cis isomer is kinetically stabilized by an activation barrier of 85−100 kJ/mol.

The mechanism of isomerization is wavelength dependent and involves rotation or inversion.[33] If the rotation mechanism is the main one in isomerization, a free volume of 0.25 nm^3 is required to allow the change.[34] In going from the linear trans isomers to the bent cis isomers, for an unsubstituted azobenzene the distance between the *para*-carbon atoms decreases from 9 to 5.5 Å and the dipole moment increases from zero to 3.0 D.[35]

Fluorescence from azobenzene in organic solvents was not detectable at room temperature. Only at low temperature and at low pH was a very weak fluorescence, having a maximum of ∼500 nm, detected by Rau.[20] Recently, two research groups reported fluorescence from azobenzene in a restricted environment (i.e., microporous aluminophosphate),[36,37] with a maximum near that reported by Rau at low pH. Shimomura and Kunitake,[23] however, found a different type of fluorescence in bilayer membranes containing azobenzene with a maximum at 600 nm, which is very similar to the maximum found here. They attributed this emission to fluorescence from an excitonic state of aggregated azobenzenes in a bilayer system where the photoisomerization of the azobenzene unit is hindered to some extent.

Comparison of the absorption (Figure 4) and emission spectra (Figures 4, 11, and 12) of the vesicles with those found in the literature for assembled azobenzenes[23,24,38] suggests that the azobenzene moieties are packed in a quite heterogeneous fashion. The absorption maximum is located at 310 nm. A broad tail extends up to 480 nm and has several shoulders (340, 355, and 375 nm). These additional bands might indicate the presence of monomeric azobenzenes and aggregates. The maximum at 310 nm corresponds to values found in the literature for H-aggregates.[23,24] There is also a very weak absorption at 450 nm, which can be attributed a forbidden $n-\pi^*$ transition. In the emission spectrum, the broad band centered at 600 nm can be assigned to the emission from aggregates.[23] The emission spectra of vesicles formed in solutions of pH 1 or 5.5 are similar and resemble the emission spectrum of a bulk dispersion of vesicles, as can be seen from Figures 11 and 12 (curves □) and Figure 4. This result indicates that the inner bilayer structure of the spherical vesicles is very similar under these conditions, as both give identical emission spectra.

The emission spectra recorded after the enhancement experiments (Figures 11 and 12, curves ○, △, and ◇), however, show a striking difference. The spectrum recorded in a pH 1 solution clearly shows a blue shift after the enhancement (Figure 11), with an intensity increase centered at 530 nm. This result is in good agreement with the spectrum of azobenzene chromophores with protonated nitrogen atoms in solution or in microporous $AlPO_4$-5.[20,23,36,37,39] This blue shift is observed only to a lesser extent in solutions of pH 5.5 (Figure 12), so this shift can be attributed to the presence of a high concentration of protons or positive charges in the proximity of the azobenzene units. A change in morphology may induce the shielded-layer structure to open, leading to close contact of part of the azobenzenes and protons from the protonated poly(propylene imine) core. Another alternative is an intrusion of protons from the intercalated water layers.

The enhanced fluorescence intensity may be caused by the arrangement of a greater amount of azobenzene moieties in a layered structure or by a change in the type of stacking of the azobenzene chromophores. The latter is quite probable as stacked azobenzenes in a head-to-tail configuration possess a higher quantum yield of fluorescence than those in a parallel configuration.[23] These changes are implied by trans−cis and cis−trans photoisomerizations of the mobile azobenzenes, producing sterical pressure and electronic interactions that might force changes in the local structure of the bilayer.

The fluorescence enhancement continues after storage of the vesicle in the absence of light. In all experiments, the fluorescence intensity reached a maximum after ∼2 h. Storage overnight did not affect the intensity further; that is, both transmission and fluorescence images remained unaltered. The intensity increase in the absence of light is probably caused by a continuing cis−trans back-isomerization to the thermodynamically more stable trans form of azobenzene. During this process, a more fluorescent type of aggregate is formed, resulting in the rise in intensity.

Additional evidence for photoisomerization in these vesicles can be obtained from the absorption spectra. After irradiation at 365 or 420 nm, a change in the absorption spectrum was observed: an increase in the absorption at 450 nm and a decrease of the absorbance at 315 nm occurred. The increased band at 450 nm can be attributed to the allowed $n-\pi^*$ transition of cis azobenzenes, proving that in these vesicles, isomerization is still possible (data not shown).

Conclusions

Poly(propylene imine) dendrimers form giant vesicles in aqueous solution. Their size distribution and structure are determined by the substituents of the dendrimer and the pH of the solution. Transmission microcopy and confocal fluorescence microscopy images have shown that these dendrimers assemble to form giant vesicles in aqueous dispersions. The stabilizing factors in these micrometer-sized objects are hydrogen bonds between protonated cores of the dendrimers (at pH < 8) and the $\pi-\pi$ stacking of the azobenzene moieties. The presence of the latter can be concluded from the emission of the vesicles, implying the presence of aggregated azobenzenes. The formation of these large aggregates is kinetically controlled, (i.e., the packing of the liquid−crystalline azobenzene units is not

(30) Eich, M.; Wendorff, J. H.; Reck, B.; Ringsdorf, H. *Makromol. Chem. Rapid Commun.* **1987**, *8*, 59−63.
(31) Natansohn, A.; Rochon, P.; Gosselin, J.; Xie, S. *Macromolecules* **1992**, *25*, 2268−2273.
(32) Rau, Von H. In *Photochromism*; Dürr, H., Bouas-Laurent, H., Eds.; Elsevier: New York, 1999.
(33) Shen, Y. Q.; Rau, Von H. *Makromol. Chem.* **1991**, *192*, 945−957.
(34) Naito, T.; Horie, K.; Mita, I. *Macromolecules* **1991**, *24*, 2907−2911.
(35) Delang, J. J.; Robertson, J. M.; Woodward, I. *Proc. R. Soc. London, Sect. A* **1939**, *171*, 398.
(36) Lei, Z.; Vaidyalingam, A.; Dutta, P. K. *J. Phys. Chem. B* **1998**, *102*, 8557−8562.
(37) Tung, C.-H.; Guan, J.-Q. *J. Org. Chem.* **1996**, *61*, 9417−9421.
(38) Shimomura, M.; Kunitake, T. *Chem. Lett.* **1981**, 1001−1004.
(39) Rau, Von H. *Ber. Bunsen-Ges. Phys. Chem.* **1971**, *75*, 1343−1347.

optimal). The vesicles can be directed to a more equilibrated mode of aggregation using a high density of photons, inducing cis−trans isomerization, followed by relaxation to an energetically more favorable configuration.

The emission spectra of isolated vesicles show that irradiation with laser light induces morphological changes. The pH dependence of the blue shift in the emission spectra shows that the vesicles are protonated to a higher degree only after illumination. Temporal distortion of the stacked azobenzene units rearranges the morphology of the bilayer structure and makes it permeable to protons.

Experimental Section

Sample Preparation. Compounds **1**−**3** were prepared according to literature procedures.[12,40] THF (Aldrich, spectrophotometric grade) was used as received. D_2O (99.9%, ACROS) and titrisol buffer (Merck) were filtered over Millex-VV Millipore filters (0.1 μm-pore size). Water used for all experiments was obtained from a Millipore Milli Q system.

The dendrimer (5 mg) was dissolved in 100 μL of THF and injected in 10 mL of hot (60−70 °C) water or 10 mL of a hot tritisol buffer (pH = 1). After cooling of the opaque dispersion, a few droplets were placed on a cover glass and used in microscopy experiments.

(40) The dendrimer is functionalized by the reaction of the end-groups with activated, pentafluorophenol esters of both palmitoy and aliphatic chains containing azobenzene moieties in the desired ratio. All products were characterized by nuclear magnetic resonance spectroscopy (NMR) and matrix-assisted laser desorption ionization time of flight mass spectroscopy (MALDI-TOF MS).

General Methods. The UV absorption spectra were recorded on a Perkin-Elmer lamda-6 UV/VIS spectrophotometer. Steady-state fluorescence emission and excitation spectra were measured on a Spex Fluorolog.

Microscopy Setup. Microscopy images were obtained using a BioRad MRC 600 beam-scanning unit, connected to a Nikon Diaphot 300 inverted microscope. Detailed information about the setup can be found elsewhere.[4, 21] All experiments were performed employing the same excitation power of $P = 25$ kW cm^{-2} and excitation wavelength of $\lambda_{ex} = 420$ nm, and $P = 250$ MW cm^{-2} for the 1064 nm light. The objective lens used in these experiments is a 100×/1.3 N. A. oil immersion lens (Zeiss Fluar).

Small-Angle X-ray Experiments. SAXS measurements were performed at the beamline ID1 of the European Synchrotron Radiation Facility (ESRF) in Grenoble, using a wavelength of 0.992 Å (12.5keV).

Acknowledgment. K.T. thanks the Mitsubishi Paper Mills Company. T.G., J.H., and L.L. thank the European Commission for a TMR fellowship within the frame of the Marie Curie program, the FWO, and the Flemish Ministry of Education, respectively. Furthermore, this work was supported by DWTC (Belgium) through IUAP-IV-11, and by ESF through SMARTON. An unrestricted research grant of DSM Research is highly appreciated.

JA9919581